J. Mol. Biol. (1993) **230**, 364–372

Analysis of the Backbone Dynamics of Interleukin-8 by ^{15}N Relaxation Measurements

Bruce L. Grasberger, Angela M. Gronenborn and G. Marius Clore

Laboratory of Chemical Physics, Building 2
National Institutes of Diabetes and Digestive and Kidney Diseases
National Institutes of Health, Bethesda, MD 20892, U.S.A.

(Received 30 September 1992; accepted 11 November 1992)

The backbone dynamics of the cytokine interleukin-8, a symmetric homodimer of overall molecular mass 16 kDa, has been investigated at pH 5·2 by means of ^{15}N relaxation measurements using heteronuclear two-dimensional inverse detected ^{1}H-^{15}N spectroscopy. ^{15}N T_1, T_2 and NOE data were obtained for 66 out of a total of 67 backbone amide groups. The overall correlation time is 9·10(±0·05) ns at 26·6 °C. All residues exhibit very rapid motions on a time-scale of ≤20 ps. These very rapid motions alone can account for the ^{15}N relaxation behaviour of 30 residues. The ^{15}N relaxation data for another 21 residues can only be accounted for by the inclusion of an additional internal motion on a time-scale ranging from 0·5 to 3·5 ns. These residues are clustered at the N and C termini, and in the loop regions connecting elements of secondary structures. Finally, the ^{15}N relaxation data for another 15 residues could only be accounted for by the presence of chemical exchange on a time-scale ranging from ~170 ns to 2·25 ms. In addition, the inclusion of chemical exchange improved the fit to the experimental data for 10 of the 30 residues whose ^{15}N relaxation behaviour could be accounted for by very fast motions alone. The residues exhibiting chemical exchange line broadening cluster at the interface of the long C-terminal α-helix and the underlying β-sheet. It is suggested that this clustering is indicative of concerted rather than independent motions in regions of secondary structure, with motion at any one residue being propagated to neighbouring residues in van der Waals contact.

Keywords: interleukin-8; protein dynamics; heteronuclear relaxation

Protein mobility plays a key role in protein–ligand interactions and protein–protein recognition (Ringe & Petsko, 1985). One method of studying protein motion involves the analysis of nuclear magnetic resonance (NMR†) relaxation processes (Lipari & Szabo, 1982). With the advent of inverse detection methods, it has now become possible to analyse the backbone dynamics of proteins on a residue by residue basis by means of ^{15}N relaxation measurements (Kay *et al.*, 1989*a*; Clore *et al.*, 1990*a*,*b*; Barbato *et al.*, 1992; Kördel *et al.*, 1992; Powers *et al.*, 1992; Stone *et al.*, 1992). In this communication we present an analysis of the backbone dynamics of the cytokine interleukin-8 (IL-8), a protein whose structure we have previously solved by both NMR and X-ray crystallography (Clore *et al.*, 1990*c*; Baldwin *et al.*, 1991; Clore & Gronenborn, 1991*a*,*b*, 1992).

IL-8 is a 16 kDa homodimer, each subunit comprising 72 residues, released from several cell types in response to an inflammatory stimulus and is associated with the selective capacity to attract neutrophils, basophils and T cells (Matsushima & Oppenheim, 1989). The overall structure of IL-8 consists of two anti-parallel α-helices, separated by about 15 Å (1 Å = 0·1 nm), lying on top of a six-stranded anti-parallel β-sheet, with a topology (Clore *et al.*, 1990*c*) reminiscent of that of the α1/α2 domains of the HLA class I histocompatibility antigen (Bjorkman *et al.*, 1987). Recent studies employing synthetic analogues (Clark-Lewis *et al.*, 1991), mutagenesis (Hebert *et al.*, 1991) and molecular modelling (Clore & Gronenborn, 1991*a*,*b*, 1992; Gronenborn & Clore, 1991) have suggested that the N terminus, the loop from residues 31 to 36 and possibly the cleft between the two helices are involved in receptor binding. The analysis of the dynamic behaviour of free IL-8 may therefore yield insights into understanding its binding to and activation of its cell surface receptors. In addition, IL-8 provides the first example of a ^{15}N relaxation study on a dimer.

† Abbreviations used: NMR, nuclear magnetic resonance; IL-8, interleukin-8; NOE, nuclear Overhauser enhancement; S.D., standard deviation; r.m.s., root-mean-square; r.m.s.d., root-mean-square difference.

0022-2836/93/060364 09 $08.00/0

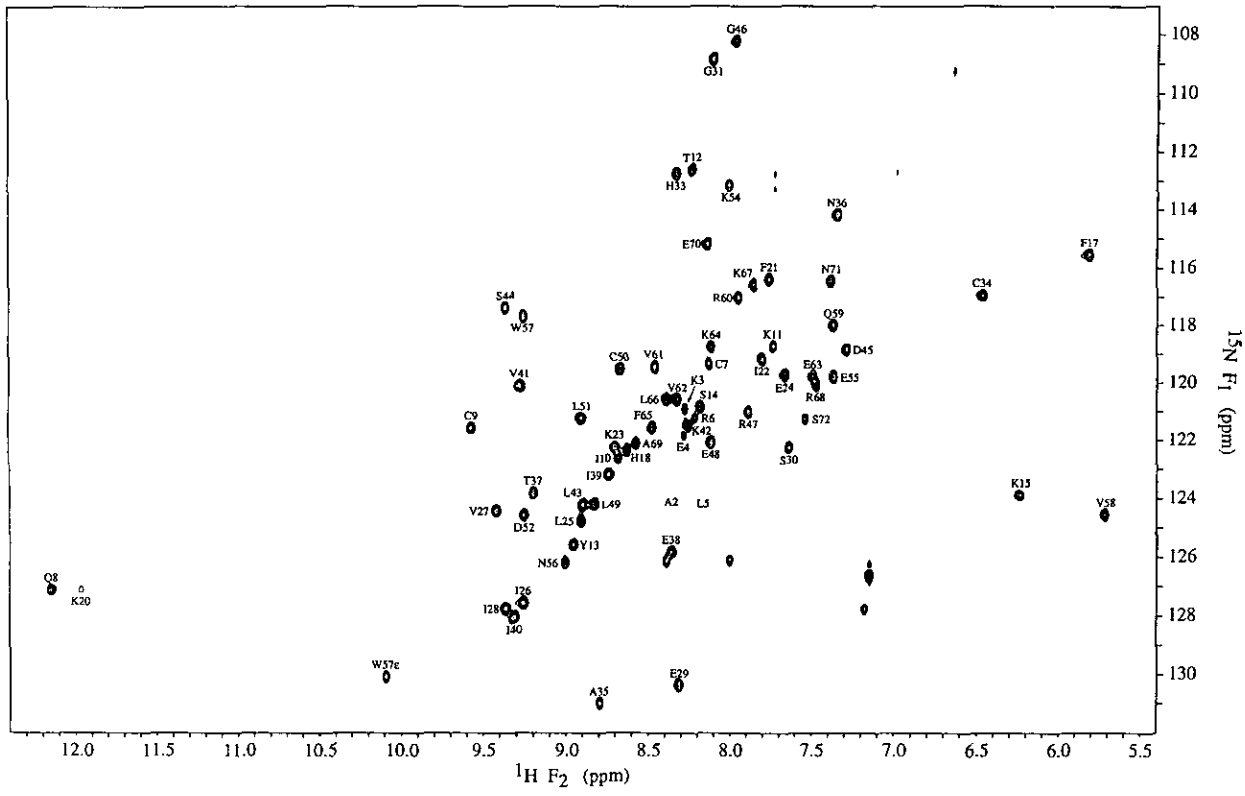

Figure 1. A 600 MHz ^{15}N-^{1}H NOE correlation spectrum of IL-8. The negative NOE peaks for Lys3 and Glu4 are shown as filled-in contours. The NOE peaks for Ala2 and Leu5 are near zero and hence cannot be observed at the contour level plotted; their location, however, is indicated. Recombinant human IL-8 was expressed in *Escherichia coli* as described (Furuta *et al.*, 1989). Uniform (>95%) ^{15}N labelling was achieved by growing the bacteria in minimal medium containing $^{15}NH_4Cl$ as the sole nitrogen source. The protein was purified from inclusion bodies as follows: after breaking the cells, the lysate was centrifuged and the pellet was washed with 1% (v/v) Triton X100, 0·75 M-urea and resuspended in 6 M-guanidine. IL-8 was refolded by sequential dialysis against 50 vol. of 3 M-urea, 2 M-urea, and finally 20 mM-$NaHPO_4$ (pH 6·5). The precipitates were collected and redissolved in guanidine for greater recoveries. The refolded protein was purified on a Mono-S FPLC (Pharmacia) column, followed by high pressure liquid chromatography on a C4 column. The sample for NMR contained ~1·5 mM-IL-8 in 90% H_2O/10% $^{2}H_2O$ (pH 5·2). All NMR data were collected at 26·6 °C on a Bruker AM600 spectrometer operating in reverse mode. The ^{15}N assignments were made on the basis of the previously assigned ^{1}H resonances (Clore *et al.*, 1989) and three-dimensional ^{15}N-separated Hartman-Hahn (Marion *et al.*, 1989) and ROESY (Clore *et al.*, 1990*d*) spectra. The ^{15}N relaxation data were measured using pulse sequences described previously (Kay *et al.*, 1989*a*; Clore *et al.*, 1990*a*) appropriately modified in the case of the ^{15}N T_1 and T_2 experiments to eliminate cross-relaxation between dipolar and chemical shift anisotropy relaxation mechanisms (Boyd *et al.*, 1990; Kay *et al.*, 1992; Palmer *et al.*, 1992). The ^{15}N T_1 and T_2 experiments were recorded with a sweep width of 5000 Hz in the ^{1}H F_2 dimension, with the carrier set to the centre of the amide NH region and the water resonance on the right-hand edge of the spectrum, using low power DANTE-style off-resonance irradiation (Kay *et al.*, 1989*b*) to suppress the water resonance. The ^{15}N-^{1}H NOE experiments were recorded with a sweep width of 10,000 Hz in the ^{1}H F_2 dimension using conventional low power irradiation to suppress the water resonance located in the centre of the spectrum. A total of 256 t_1 increments, each of 1024 data points for the ^{15}N T_1 and T_2 experiments, and 2048 data points for the ^{1}H-^{15}N NOE experiments, were recorded, giving a total acquisition time in t_1 of 40·4 ms and a spectral width of 1582 Hz in the ^{15}N F_1 dimension. 32 transients/increment were recorded for the ^{15}N T_1 and T_2 experiments and 136 transients/increment for the ^{1}H-^{15}N NOE experiments. The recycle time was 1·2 s for the ^{15}N T_1 and T_2 experiments and 3 s for the ^{1}H-^{15}N NOE experiments. ^{15}N T_1 data were obtained for 9 T delays of 12·1, 20·2, 36·3, 84·8, 165·6, 327·2, 529·2, 731·2 and 1054·3 ms, and ^{15}N T_2 data for 7 T delays of 14·4, 28·7, 57·5, 114·9, 172·4, 229·9 and 237·3 ms. All NMR data were processed using NMR2 software (New Methods Research, Syracuse, NY, U.S.A.) and analysed with the programs PIPP and CAPP (Garrett *et al.*, 1991) running on a Sun Sparc workstation. In the F_2 dimension, a linear baseline correction was applied for the ^{15}N T_1 and T_2 data and a polynomial baseline correction of order 3 for the NOE data. The decay of cross-peak intensities with time in the ^{15}N T_1 and T_2 experiments is exponential within experimental error, and the decays were fit to a single exponential by non-linear least-squares Powell minimization using the program FACSIMILE (Chance *et al.*, 1979; Clore, 1983). The errors in the T_1 and T_2 values were obtained from conventional analysis of the variance-covariance matrix generated by the non-linear least-squares optimization routine (Chance *et al.*, 1979; Clore, 1983). Out of the 66 amide groups for which T_1 and T_2 values were obtained, 63 T_1 values had errors ≤5%, 2 T_1 values (Thr12 and Ile40) had errors between 5 to 10%, and 1 T_1 value (Ser14) had an error of 13%; 54 T_2 values had an error of ≤5%, 11 T_2 values (Ala2, Tyr13, Ser14, Lys15, His18, Val27, Gly31, Cys34, Glu38, Ile39 and Ile40) had errors of 5 to 10%, and 1 T_2 value had an error of ~12% (Ser30). The error in the experimental measurement of the ^{1}H-^{15}N NOE was of the order of ±0·1. It should be noted that there is also a potential systematic error in the measurement of the ^{15}N-^{1}H NOE arising from chemical exchange with water; for a T_1 of ~2·5 s for water and a recycle

The ^{15}N relaxation data were measured using pulse sequences described previously (Kay *et al.*, 1989*a*; Clore *et al.*, 1990*a*) taking care to eliminate cross-correlation between dipolar and chemical shift anisotropy relaxation mechanisms (Boyd *et al.*, 1990; Kay *et al.*, 1992; Palmer *et al.*, 1992). ^{15}N T_1 and T_2 data were obtained for all backbone amide nitrogen atoms with the exception of Gln20 (for which the cross-peak was too weak to obtain reliable relaxation times), and ^{15}N NOE data were obtained for all backbone amide groups. The ^1H-^{15}N NOE correlation spectrum is shown in Figure 1, and the ^{15}N T_1, T_2 and NOE values are plotted as a function of residue number in Figure 2A to C.

The overall rotational correlation time, τ_R, was calculated from the T_1/T_2 ratios, excluding those residues with a T_1/T_2 ratio outside one standard deviation of the mean, as described by Clore *et al.* (1990*a*). The mean T_1/T_2 ratio for the amide nitrogen atoms of IL-8 was 8·52(±1·62) with a maximum of 10·85 for His18 and a minimum of 3·05 for Glu4. Ala2, Lys3, Glu4, Leu5, Arg6 and Ser72 have T_1/T_2 ratios of <6·90, implying a significant degree of internal motion. His18, Asp52, Val61 and Val62 have T_1/T_2 ratios of >10·14, indicative of chemical exchange line broadening. The average T_1/T_2 of the remaining 56 residues is 8·59(±1·54), and the calculated τ_R obtained by fitting the T_1/T_2 ratios of these residues simultaneously is 9·10(±0·05) ns.

Of the 51 residues which did not require any contribution from chemical exchange to account for their ^{15}N relaxation data, the T_1 and T_2 data of 30 residues, all with NOE values >0·7, could be adequately fitted (i.e. within ±1 S.D.) by the simplified spectral density function of Lipari & Szabo (1982):

$$J(\omega_i) = S^2\tau_R/(1+\omega_i^2\tau_R^2), \quad (1)$$

in which terms containing the internal correlation time τ_e are neglected (i.e. τ_e is ≤20 ps and hence makes a negligible contribution to T_1 and T_2). The order parameter S^2 for these 30 residues is ≥0·8, indicating restricted internal motion. The remaining 21 residues in this group either had NOE values ≤0·7 or their ^{15}N T_1 and T_2 data could not be accounted for by equation (1) (i.e. the calculated T_1 and/or T_2 values lie outside ±1 S.D. of the corresponding experimental values). The ^{15}N T_1, T_2 and NOE relaxation data for these 21 residues could not be fitted by the complete Lipari & Szabo (1982) model free spectral density function:

$$J(\omega_i) = S^2\tau_R/(1+\omega_i^2\tau_R^2)+(1-S^2)\tau_e'/(1+\omega_i^2\tau_e'^2), \quad (2)$$

where $\tau_e' = \tau_R\tau_e/(\tau_R+\tau_e)$. Specifically, equation (2) predicted significantly smaller NOE values than observed (see Clore *et al.*, 1990*a*,*b*). As in previous examples (Clore *et al.*, 1990*a*,*b*; Powers *et al.*, 1992; Barbato *et al.*, 1992), the ^{15}N relaxation data for these residues could only be accounted for by the extension of the Lipari & Szabo (1982) model described by Clore *et al.* (1990*b*) in which the internal motions inside (fast) and outside (slow) the extreme narrowing limit are distinct with rates for the two regions differing by at least an order of magnitude (i.e. $\tau_f < 20$ ps, 200 ps $< \tau_s < \tau_R$). This is described by the spectral density function:

$$J(\omega_i) = S^2\tau_R/(1+\omega_i^2\tau_R^2)+S_f^2(1-S_s^2)\tau_s'/(1+\omega_i^2\tau_s'^2), \quad (3)$$

where S_f^2 and S_s^2 are the order parameters for the fast and slow motions, τ_s is the internal correlation time for the slow motions (with $\tau_s' = \tau_R\tau_s/(\tau_R+\tau_s)$). τ_f, the internal correlation time for the fast motions, is assumed to be ≤20 ps so that terms containing τ_f are neglected. The values obtained for τ_s and S_s^2 range from 0·5 to 3·5 ns and from 0·2 to 0·9, respectively, while S_f^2 is >0·8.

The relaxation data for the other 15 residues could only be accounted for by including an exchange line broadening term Δex for T_2:

$$1/T_2(\text{obs}) = 1/T_2+\pi\Delta\text{ex}. \quad (4)$$

The lifetime for the chemical exchange processes can be estimated to lie between 170 ns and 2·25 ms (Powers *et al.*, 1992). The ^{15}N relaxation data for all but two of these residues could then be accounted for by equation (1). The ^{15}N relaxation data for Thr37 and Arg68, however, could only be accounted for by equation (2) and chemical exchange. The internal correlation times τ_e for these two residues (51 and 68 ps, respectively) indicate that in addition to a slow chemical exchange process, their NH vectors undergo some motions that are slower than the ubiquitous fast thermal motions described by equation (1), but still located in the extreme narrowing limit. In addition, there were another ten residues whose ^{15}N relaxation data could be fitted slightly better to equation (1) plus chemical exchange than to equation (1) alone.

The results of the analysis of the relaxation data are shown in Figure 2 and the location in the three-dimensional structure of IL-8 of the residues exhibiting the various types of relaxation behaviour is depicted in Figure 3.

Excluding the residues 2 to 6 and 72 at the N and C termini, respectively, the average value of the overall order parameter S^2 is 0·87(±0·06) with a

time of 3 s, this effect may result in a systematic increase of at most 20% in the absolute value of the ^{15}N-^1H NOE (Clore *et al.*, 1990*a*) and probably accounts for the observation that in a few cases the measured ^{15}N-^1H NOE value was greater than the theoretical maximum of 0·82. In such cases, a value of 0·82(±0·1) was assumed for fitting the data to various spectral density functions. (It should be noted that the 5 unlabelled cross-peaks between $\delta^{15}N = 126$ to 128 parts per million probably represent folded peaks arising from interactions *via* 2-bond J couplings between the nitrogen atoms and non-exchangeable protons of the imidazole ring of the 2 histidine residues; they were not observed in the regular 2-dimensional ^1H-^{15}N Overbodenhausen correlation spectrum, in the ^{15}N T_1 and T_2 experiments, or in the 3-dimensional ^{15}N-separated HOHAHA and ROESY spectra.)

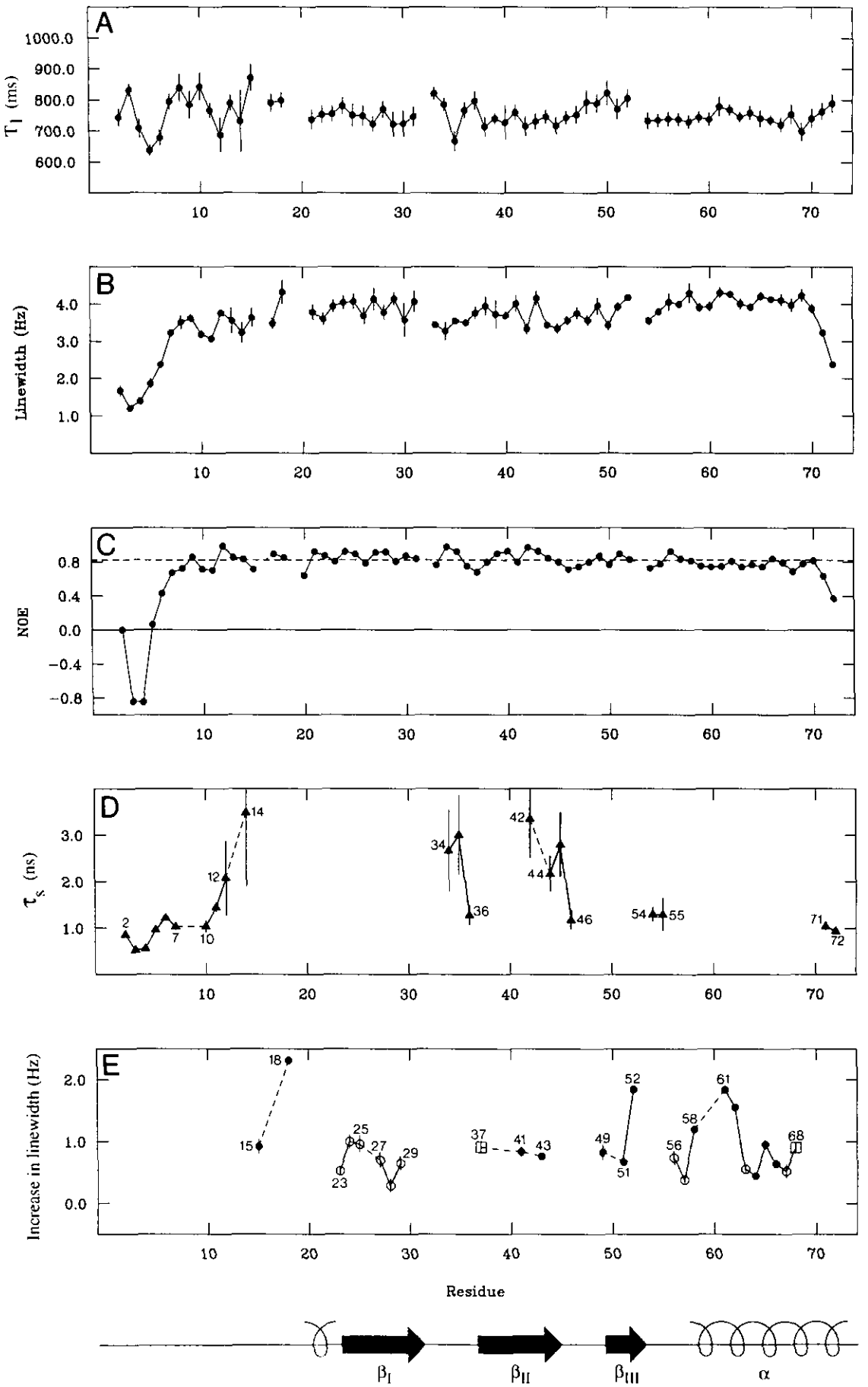
A
T_1 (ms)
1000.0
900.0
800.0
700.0
600.0
B
Linewidth (Hz)
4.0
3.0
2.0
1.0
C
NOE
0.8
0.4
0.0
−0.4
−0.8
D
τ_s (ns)
3.0
2.0
1.0
2
7
10
12
14
34
36
42
44
46
54
55
71
72
E
Increase in linewidth (Hz)
2.0
1.0
0.0
15
18
23
25
27
29
37
41
43
49
51
52
56
58
61
68
10
20
30
40
50
60
70
Residue
β_I
β_{II}
β_{III}
α

Fig. 2.

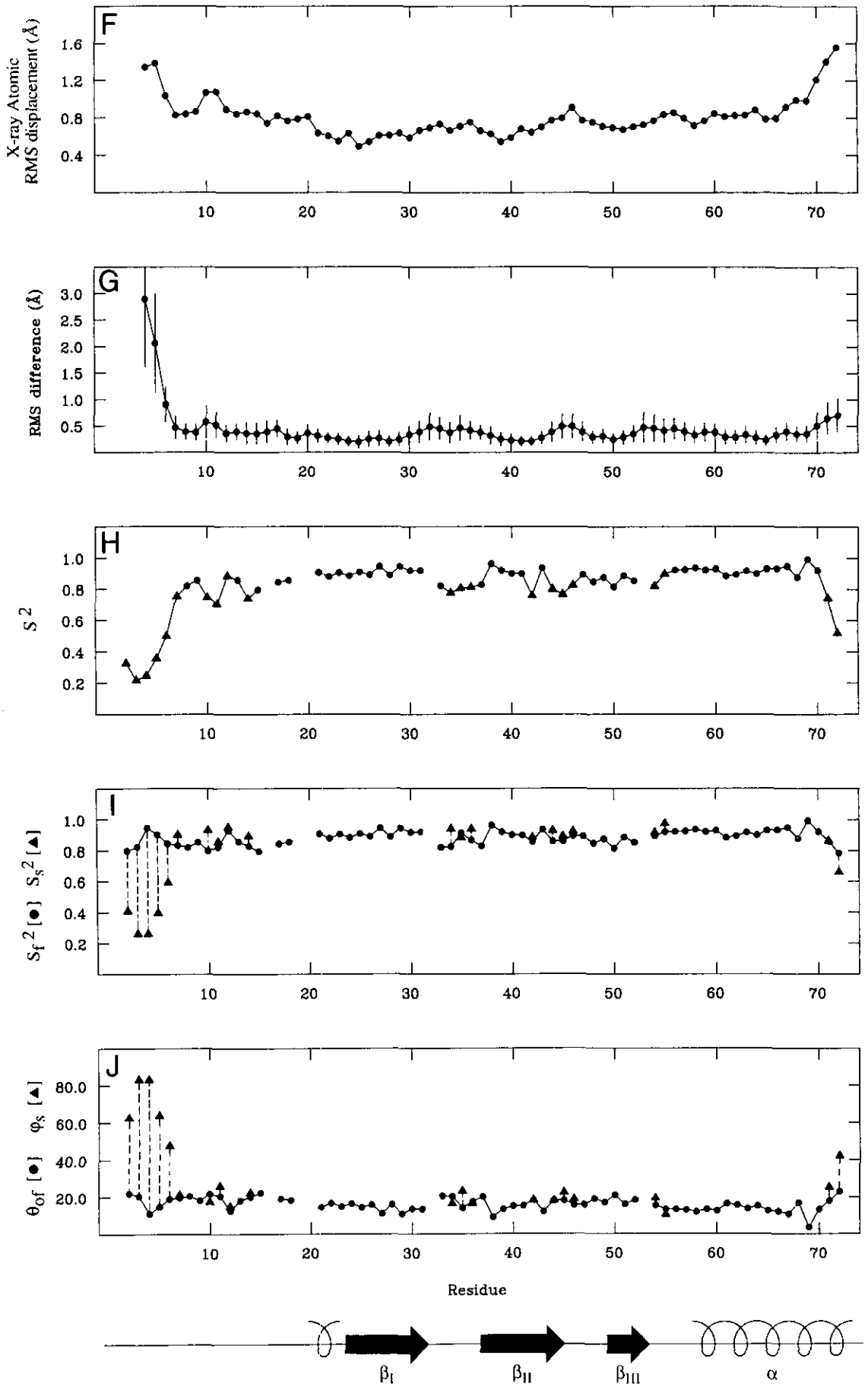
F
X-ray Atomic RMS displacement (Å)
1.6
1.2
0.8
0.4
10
20
30
40
50
60
70
G
RMS difference (Å)
3.0
2.5
2.0
1.5
1.0
0.5
H
S^2
1.0
0.8
0.6
0.4
0.2
I
S_f^2 [●] S_s^2 [▲]
J
θ_{Of} [●] φ_S [▲]
80.0
60.0
40.0
20.0
Residue
β_I
β_{II}
β_{III}
α

Fig. 2.

range spanning from 0·70 to 0·99, indicating that IL-8 is a fairly rigid molecule. The average value for S_f^2 (which is equal to S^2 in the case of those residues whose relaxation data can be fitted to eqn (1)) is 0·88(±0·05), which is equivalent to free diffusion within an axially symmetric cone of semiangle $\phi_{of} = 17{\cdot}4(\pm 4{\cdot}3)°$. All these values are comparable to those found in previous studies (Clore *et al.*, 1990*a*).

Residues whose relaxation behaviour can be accounted for by the simplified Lipari & Szabo (1982) correlation function (eqn (1)) alone are, in general, located in regions of hydrogen bonded structure (e.g. the single 3_{10} helical turn from residues 19 to 22, which is also stabilized by a hydrogen bond from the backbone amide group of Lys20 to the $N^{\delta 1}$ imidazole atom of His18, the turn comprising residues 30 to 33, which connects β-strands 1 and 2 and is stabilized by 2 hydrogen bonds, residues 47 to 50 located in β-strand 3 in the vicinity of the disulphide bond between Cys9 and Cys50, and residues 59, 60, 69 and 70 in the C-terminal helix).

The residues at the N and C termini exhibit a high degree of mobility with the overall order parameter S^2 ranging from 0·2 to 0·6. These residues all require the presence of two internal motions (i.e. eqn (3)). Interpreting the order parameter S_s^2 for the slow motions in terms of a two-state jump model on the nanosecond time-scale (Clore *et al.*, 1990*a*) yields an angle φ_s between the NH vectors in the two states ranging from 48° to 83°. A number of other residues, located either at the N terminus (residue 7), the C terminus (residue 71), in loop regions (residues 10 to 12 and 14), in turns connecting β-strands (residues 34 to 36 between β-strands 2 and 3, and residues 42 and 44 to 46 between β-strands 3 and 4) or in the turn connecting β-strand 4 to the C-terminal helix (residues 54 to 55), reveal the presence of slow internal motions on a time-scale ranging from 1 to 3·5 ns and display lower than average overall order parameters S^2. The lack of secondary structure allows these residues to move more independently since they are located on the surface of the molecule and are not restricted by packing within the hydrophobic core.

It is interesting to note that in the long series of N-terminal residues whose relaxation data is described by equation (3), a break occurs at residues 8 and 9. The internal motions in this short stretch are, in all likelihood, restricted by the interaction between the backbone amide proton of Gln8 and the imidazole ring of His33 (Clore *et al.*, 1990*c*) and by the disulphide bridge between Cys9 and Cys50 (located in the middle of β-strand 4). This contrasts with the situation at the second disulphide bond formed by Cys7 and Cys34, where both residues exhibit the additional slow internal motion, presumably due to the fact that Cys34 is located in a loop region.

A comparison of the crystallographic atomic root-mean-square (r.m.s.) displacements for the backbone nitrogen atoms derived from the *B*-factor values (Fig. 2F), the root-mean-square difference (r.m.s.d.) of the calculated NMR structures about their mean co-ordinate positions (Fig. 2G), and the overall order parameter S^2 (Fig. 2H) indicates some degree of correlation between these three parameters. This is also depicted by the correlation plot and regression analysis shown in Figure 4. Not surprisingly, the correlation between S^2 and the NMR r.m.s.d. (correlation coefficient $= -0{\cdot}86$) is significantly better than that between S^2 and the X-ray atomic r.m.s. displacements (correlation coefficient $= -0{\cdot}69$). This is mainly due to the fact that, although the mobility of residues 4 to 6 in the X-ray structure is higher than average, they are still relatively well ordered on account of a salt bridge

Figure 2. Plots as a function of residue of: A, ^{15}N T_1; B, ^{15}N T_2 (displayed as linewidth $= 1/(\pi T_2)$); C, ^{15}N-^1H NOE values measured at 600 MHz; D, values calculated from the data of τ_s for residues fit to eqn (3); E, the exchange linewidth for residues fit to eqns (1) and (4) (filled circles, or open circles for those residues that can also be fit to eqn (1) alone) and for residues fit to eqns (2) and (4) (open squares); H, the overall order parameter S^2 (filled circles for residues fitting eqns (1) or (2) with or without exchange line broadening; filled triangles for residues fitting eqn (3)); I, the fast S_f^2 (circles) and slow S_s^2 (triangles) motion order parameters. In J, the values of the θ_{of} (circles) and φ_s (triangles) angles given by $S_f^2 = (0{\cdot}5 \cos\theta_{of}(1 + \cos\theta_{of}))^2$ and $S_s^2 = (1 + 3\cos^2\varphi_s)/4$, respectively, are displayed for residues whose relaxation behaviour is described by eqn (3); in this interpretation of the motions described by the spectral density function eqn (3), the slower motion is represented by a jump between 2 states, *i* and *j*, while the faster motion is represented as free diffusion within 2 axially symmetric cones centred about the 2 states, *i* and *j*; θ_{of} is the semi-angle of the cone, while φ_s is the angle between the NH vectors in the 2 states, *i* and *j* (Clore *et al.*, 1990*a*). Also shown are F, the crystallographic atomic r.m.s. displacements, $\langle r^2\rangle^{1/2}$, for the backbone nitrogen atoms calculated from the Debye–Waller *B*-factor values ($\langle r^2\rangle^{1/2} = (3B/8\pi^2)^{1/2}$) (Baldwin *et al.*, 1991); and G, the average r.m.s. difference of the backbone nitrogen atoms of the 30 individual calculated NMR structures about the mean co-ordinate positions (Clore *et al.*, 1990*c*). The FACSIMILE program (Chance *et al.*, 1979; Clore, 1983) was used to analyse the relaxation data as described previously (Clore *et al.*, 1990*a*,*b*). The fitting procedure takes into account the experimental errors in the ^{15}N relaxation data, and the errors in the values of the optimized parameters are obtained from analysis of the variance-covariance matrix. In fitting the experimental relaxation data to various functions, a fit to a given function is considered inadequate when 1 or more of the calculated relaxation parameters (i.e. T_1, T_2 or NOE) lies outside ±1 S.D. of the corresponding experimental value. The standard deviations of the experimental T_1 and T_2 data and of the calculated motional parameters are indicated by vertical bars. It should be noted that the errors for the calculated order parameters (S^2, S_s^2 and S_f^2), which range from 0·1 to 2%, with the majority being less than 0·5%, are smaller than the symbols. (The same is also true for some of the calculated values of Δex). A schematic representation of the secondary structure is shown at the bottom of the Figure.

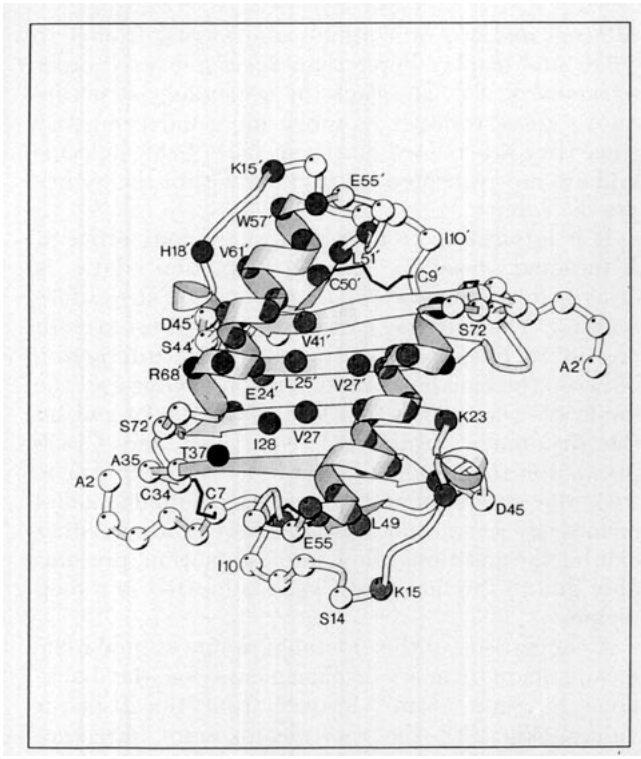

Figure 3. Ribbon diagram of the solution structure of the IL-8 dimer (Clore *et al.*, 1990*c*). The residues that fit to the spectral density function given by eqn (3) (i.e. 2 *internal motions, 1 very fast and 1 slow*) are indicated by white spheres. Residues that fit to either the simplified (eqn (1)) or full (eqn (2)) Lipari & Szabo (1982) spectral density functions in the presence of chemical exchange (eqn (4)) are indicated by grey and black spheres, respectively. This diagram was created using the program MOLSCRIPT (Kraulis, 1991). As the algorithm for generating the ribbon is based on the C^{α} atom co-ordinates, the spheres are positioned for clarity at the C^{α} atom, rather than the backbone N atom positions.

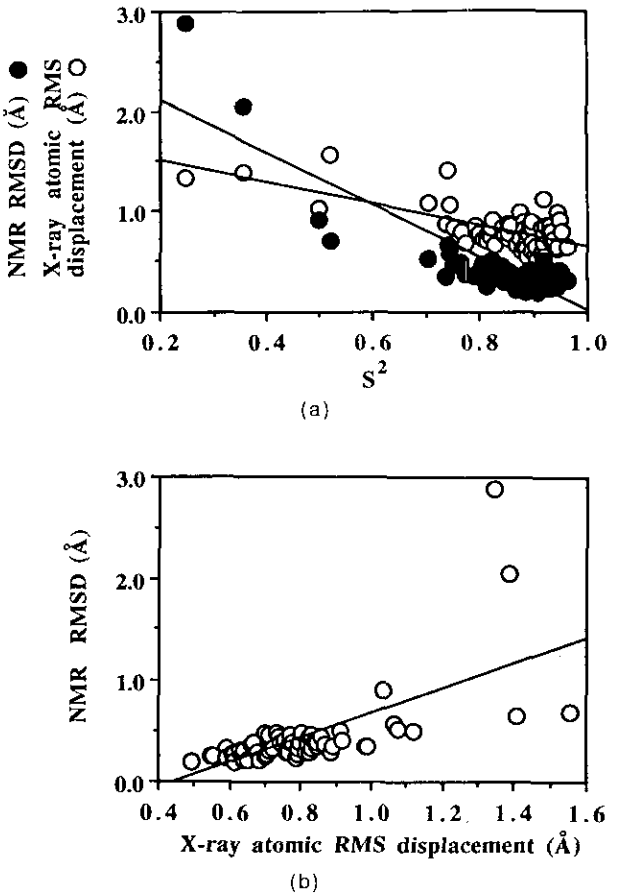

Figure 4. Correlation plot and least-squares regression analysis of (a) the generalized order parameter S^2 *versus* the r.m.s.d. of the individual calculated NMR structures about their mean co-ordinate positions (filled circles, correlation coefficient $= -0.86$) and the X-ray atomic r.m.s. displacements of the backbone nitrogen atoms (open circles, correlation coefficient $= -0.69$), and of (b) the r.m.s.d. from the NMR structures *versus* the X-ray *atomic r.m.s. displacements* (correlation coefficient $= 0.64$). The r.m.s.d. values for the calculated NMR structures and the X-ray atomic r.m.s. displacements are from Clore *et al.* (1990*c*) and Baldwin *et al.* (1991), respectively.

between the carboxylate group of Glu4 of one subunit and the $N^{\zeta}H_3^+$ of Lys23 of the other subunit (Clore & Gronenborn, 1991*a*). In contrast, residues 4 *to 6 are disordered in the solution* NMR *structures*, consistent with the absence of non-sequential ^1H-^1H NOEs (Clore *et al.*, 1989, 1990*c*; Clore & Gronenborn, 1991*a*) and the very low overall order parameters.

It should be emphasized, however, that the observed correlation between the overall order parameter S^2 and the r.m.s.d. of the calculated NMR structures is an indirect one, as the latter is directly related to the number and density of the ^1H-^1H NOE derived interproton distance restraints. Clearly, the density of short (<5 Å) interproton distance contacts in exposed regions of the protein, such as loops, will be reduced, resulting in a higher NMR r.m.s.d. Consequently, even if such a loop region were rigid, for example due to stabilization by a salt bridge, it is likely that its NMR r.m.s.d. would be high. Moreover, it should be borne in mind that the NMR r.m.s.d. is also related to the degree of refinement, and thus any inference of mobility should be restricted to high resolution fourth generation NMR structures in which over 90% of the structurally useful NOEs have been assigned (Clore & Gronenborn, 1991*b*).

Residues that exhibit exchange line broadening cluster in regions of secondary structure, especially β-strands 2 and 3, the long C-terminal α-helix and, in particular, those residues that make contact between the helix and the underlying β-sheet (Figs 2E and 3). Line broadening arises from the existence of at least two distinct species with different chemical shifts. Since these residues have mutually stabilizing hydrogen bonds and buried hydrophobic side-chains, the grouping suggests a concerted movement of the residues between two or more conformations.

Many of the residues whose ^{15}N relaxation data can be accounted for by the simplified Lipari &

Szabo (1982) correlation function (eqn (1)), together with chemical exchange (eqn (4)), are in van der Waals contact (Fig. 3). In β-strands 2 and 3, the backbone amide and carbonyl groups of Val41 and Leu49 are hydrogen-bonded and, in addition, there are contacts between the side-chains of Val41 and Leu51 and between Leu49 and Leu43. The side-chain of Val58 in the long C-terminal α-helix contacts the side-chain of Leu51 and the backbone amide group of Asp52 in β-strand 3. Contacts between residues in β-strand 1 and the overlying helix include Leu25 to Phe65, Val27 to Phe65′ (of the other subunit), and Glu29 to Phe65′ and Arg68′. In addition, the side-chain of Leu25 in β-strand 1 contacts the side-chain of Val41 in β-strand 2. Many of these contacts involve the burying of hydrophobic side-chains. It is interesting to note that the only residue in β-strand 1 that does not exhibit exchange line broadening is Arg26. This residue is located at the C_2 symmetry axis of the dimer, and therefore at the pivot point of any potential motion of the dimers relative to each other with respect to this axis. This could arise, for example, from a change in the angle between the long axes of the two central strands (i.e. strands 1 and 1′) of the β-sheet at the dimer interface. Consequently, it is likely to experience only very small (if any) ^{15}N chemical shift differences between different conformational states. That this type of motion may, indeed, occur is evidenced by the fact that the difference in the quaternary arrangement of the subunits between the solution and crystal structures can be directly attributed to a rigid body rotation of the two subunits about the C_2 symmetry axis as a result of a change in the angle between the two central strands from approximately 168° in the solution structure to approximately 179° in the crystal structure (Clore & Gronenborn, 1991*a*).

Although both Lys15 and His18 exhibit exchange line broadening, they are not located in secondary structure elements. However, the adjacent residues, Pro16 and Pro19, respectively, are in van der Waals contact with Trp57 and Phe65 in the long helix, both of which exhibit exchange line broadening. Motions of these nearby aromatic side-chains may cause changes in the ^{15}N chemical shifts of these residues. Other residues that exhibit exchange line broadening and are in contact with Pro19 include the side-chains of Val61 and Lys64 in the long helix.

Finally, there are two residues, Thr37 and Arg68, whose ^{15}N relaxation behaviour can only be accounted for by both chemical exchange and a significant contribution from internal motion (i.e. eqns (2) and (4)). While both these residues are in close proximity to other residues exhibiting exchange line broadening, they are located at the boundaries of secondary structure elements, namely at the beginning of β-strand 2 (Thr37) and at the end of the C-terminal helix (Arg68). Hence, it is perhaps not surprising that, in addition to chemical exchange, these two residues may participate in some of the same type of motions that the more mobile residues display.

The pictorial description of the ^{15}N relaxation data of IL-8 presented in Figure 3 makes it strikingly obvious that the ordered secondary structure elements exhibit a qualitative difference in dynamic behaviour from the more irregular loops and turns. Thus, whereas the residues located in the latter can move more freely and independently, a number of residues in the β-sheet and α-helices undergo motions on a time-scale longer than the rotational correlation time. The latter are in all likelihood concerted in nature since (1) the residues involved form a three-dimensional cluster, (2) both the six-stranded β-sheet and the two overlying helices in IL-8 are mutually stabilized by hydrophobic interactions at their interface (Clore *et al.*, 1990*a*), and (3) structural changes in proteins tend to be highly co-operative. It therefore seems probable that any motion in one structural unit will be propagated to the other *via* interacting residues, such that compensatory conformational changes will ensure optimal arrangements of these elements in terms of interaction energies. Such motions can involve concerted intra-domain local motions as well as rigid body motions of the two subunits relative to each other.

This work was supported by the Intramural AIDS Targeted Antiviral Program of the Office of the Director of the National Institutes of Health (G.M.C. and A.M.G.).

References

Baldwin, E. T., Weber, I. T., St Charles, R., Xuan, J. C., Appella, E., Yamada, M., Matsushima, K., Edwards, B. F. P., Clore, G. M., Gronenborn, A. M. & Wlodawer, A. (1991). Crystal structure of interleukin-8: symbiosis of NMR and crystallography. *Proc. Nat. Acad. Sci., U.S.A.* **88**, 502–506.

Barbato, G., Ikura, M., Kay, L. E. & Bax, A. (1992). Backbone dynamics of calmodulin studied by ^{15}N relaxation using inverse detected two-dimensional NMR spectroscopy: the central helix is flexible. *Biochemistry*, **31**, 5269–5278.

Bjorkman, P. J., Saper, M. A., Samraoui, B., Bennett, W. S., Strominger, J. L. & Wiley, D. C. (1987). Structure of human class I histocompatibility antigen HLA-A2. *Nature (London)*, **329**, 506–512.

Boyd, J., Hommel, U. & Campbell, I. D. (1990). Influence of cross-correlation between dipolar and anisotropic chemical shift relaxation mechanisms upon longitudinal relaxation rates of ^{15}N in macromolecules. *Chem. Phys. Letters*, **175**, 477–482.

Chance, E. M., Curtis, A. R., Jones, I. P. & Kirby, C. R. (1979). FACSIMILE: a computer program for flow and chemistry simulation, and general initial value problems. *U.K. Atomic Energy Authority, Harwell [Rep.] AERE-R 8775.*

Clark-Lewis, I., Schumacher, C., Baggiolini, M. & Moser, B. (1991). Structure-activity relationships of interleukin-8 determined using chemically synthesized analogs. *J. Biol. Chem.* **266**, 23128–23134.

Clore, G. M. (1983). Computer analysis of transient kinetic data. In *Computing in Biological Science* (Geisow, M. J. & Barrett, M., eds), pp. 313–348, Elsevier North-Holland, Amsterdam, The Netherlands.

Clore, G. M. & Gronenborn, A. M. (1991*a*). Comparison of

the solution nuclear magnetic resonance and crystal structures of interleukin-8. *J. Mol. Biol.* **217**, 611–620.

Clore, G. M. & Gronenborn, A. M. (1991*b*). Structures of larger proteins in solution: three- and four-dimensional heteronuclear NMR spectroscopy. *Science*, **252**, 1390–1399.

Clore, G. M. & Gronenborn, A. M. (1992). NMR and X-ray analysis of the three-dimensional structure of interleukin-8. In *Interleukin-8 (NAP-1) and Related Chemotatic Cytokines, Cytokines*, vol. 4, pp. 18–40, Karger, Basel.

Clore, G. M., Appella, E., Yamada, M., Matsushima, K. & Gronenborn, A. M. (1989). Determination of the secondary structure of interleukin-8 by nuclear magnetic resonance spectroscopy. *J. Biol. Chem.* **263**, 18907–18911.

Clore, G. M., Driscoll, P. C., Wingfield, P. T. & Gronenborn, A. M. (1990*a*). Analysis of the backbone dynamics of interleukin-1β using two-dimensional inverse detected heteronuclear ^{15}N-^{1}H NMR spectroscopy. *Biochemistry*, **29**, 7387–7401.

Clore, G. M., Sazbo, A., Bax, A., Kay, L. E., Driscoll, P. C. & Gronenborn, A. M. (1990*b*). Deviations from the simple two-parameter model-free approach to the interpretation of nitrogen-15 nuclear magnetic relaxation of proteins. *J. Amer. Chem. Soc.* **112**, 4989–4991.

Clore, G. M., Appella. E., Yamada, M., Matsushima, K. & Gronenborn, A. M. (1990*c*). Three dimensional structure of interleukin-8 in solution. *Biochemistry*, **29**, 1689–1700.

Clore, G. M., Bax, A., Wingfield, P. T. & Gronenborn, A. M. (1990*d*). Identification and localization of bound internal water in the solution structure of interleukin-1β by heteronuclear three-dimensional ^{1}H rotating-frame Overhauser ^{15}N-^{1}N multiple quantum coherence NMR spectroscopy. *Biochemistry*, **29**, 5671–5676.

Furuta, R., Yamagishi, J., Kotani, H., Sakamoto, F., Fukui, T., Matsui, Y., Sohmura, Y., Yamada, M., Yoshimura, T., Larsen, C. G., Oppenheim, J. J. & Matsushima, K. (1989). Production and characterization of recombinant human neutrophil chemotactic factor. *J. Biochem.* **106**, 436–441.

Garrett, D. S., Powers, R., Gronenborn, A. M. & Clore, G. M. (1991). A common sense approach to peak peaking in two-, three-, and four-dimensional spectra using automatic computer analysis of contour diagrams *J. Magn. Res.* **95**, 214–220.

Gronenborn, A. M. & Clore, G. M. (1991). Modeling the three-dimensional structure of the monocyte chemoattractant and activating protein MCAF/MCP-1 on the basis of the solution structure of interleukin-8. *Protein Eng.* **4**, 263–269.

Hebert, C. A., Vitangcol, R. V. & Baker, J. B. (1991). Scanning mutagenesis of interleukin-8 identifies a cluster of residues required for receptor binding. *J. Biol. Chem.* **266**, 18989–18994.

Kay, L. E., Torchia, D. A. & Bax, A. (1989*a*). Backbone dynamics of proteins as studied by ^{15}N inverse detected heteronuclear NMR spectroscopy: application to staphylococcal nuclease. *Biochemistry*, **28**, 8972–8979.

Kay. L. E., Marion, D. & Bax, A. (1989*b*). Practical aspects of three-dimensional heteronuclear NMR of proteins. *J. Magn. Reson.* **84**, 72–84.

Kay, L. E., Nicholson, L. K., Delaglio, F., Bax, A. & Torchia, D. A. (1992). The effects of cross-correlation between dipolar and chemical shift anisotropy relaxation mechanisms on the measurement of T_1 and T_2 values in proteins: pulse sequences for the removal of such effects. *J. Magn. Reson.* **97**, 359–375.

Kördel, J., Skelton, N. J., Akke, M., Palmer, A. G. & Chazin, W. J. (1992). Backbone dynamics of calcium-loaded calbindin D9k studied by two-dimensional proton detected ^{15}N NMR spectroscopy. *Biochemistry*, **31**, 4856–4866.

Kraulis, P. J. (1991). MOLSCRIPT: a program to produce both detailed and schematic plots of protein structures. *J. Appl. Crystallogr.* **24**, 946–950.

Lipari, G. & Szabo, A. (1982). Model-free approach to the interpretation of nuclear magnetic resonance relaxation in macromolecules. *J. Amer. Chem. Soc.* **104**, 4546–4559.

Marion, D., Driscoll, P. C., Kay, L. E., Wingfield, P. T., Bax, A., Gronenborn, A. M. & Clore, G. M. (1989). Overcoming the overlap problem in the assignment of ^{1}H NMR spectra of larger proteins using three-dimensional heteronuclear ^{1}H-^{15}N Hartmann-Hahn-multiple quantum coherence and nuclear Overhauser-multiple quantum coherence spectroscopy: application to interleukin-1β. *Biochemistry*, **28**, 6150–6156.

Matsushima, K. & Oppenheim, J. J. (1989). Interleukin-8 and MCAF: novel inflammatory cytokines inducible by IL-1 and TNF. *Cytokine*, 1, 2–13.

Palmer, A. G., Skelton, N. J., Chazin, W. J., Wright, P. E. & Rance, M. (1992). Suppression of cross-correlation between dipolar and anisotropic chemical shift relaxation mechanisms in the measurement of spin-spin relaxation rates. *Mol. Phys.* **75**, 699–711.

Peng, J. W. & Wagner, G. (1992). Mapping of the spectral densities of N–H bond motions in eglin *c* using heteronuclear relaxation experiments. *Biochemistry*, **31**, 8571–8586.

Powers, R., Clore, G. M., Wingfield, P. T., Stahl, S. J. & Gronenborn, A. M. (1992). Analysis of the backbone dynamics of the ribonuclease H domain of the human immunodeficiency virus reverse transcriptase by two-dimensional inverse detected heteronuclear NMR spectroscopy. *Biochemistry*, **31**, 9150–9157.

Ringe, D. & Petsko, G. A. (1985). Mapping protein dynamics by X-ray diffraction. *Prog. Biophys. Mol. Biol.* **45**, 197–235.

Stone, M. J., Fairbrother, W. J., Palmer, A. J., Reizer, J., Saier, M. H. & Wright, P. E. (1992). The backbone dynamics of the *Bacillus subtilis* glucose permease IIA domain determined from ^{15}N NMR relaxation measurements. *Biochemistry*, **31**, 4394–4406.

Edited by P. E. Wright